Journal of Pharmaceutical Innovation (2023) 18:2402–2418
https://doi.org/10.1007/s12247-023-09800-y

ORIGINAL ARTICLE

Exploiting response surface D-optimal design study for preparation and optimization of spanlastics loaded with miconazole nitrate as a model antifungal drug for topical application

Mervat Shafik Ibrahim[1] · Omar A. Elkady[1] · Mai A. Amer[2] · Shereen H. Noshi[1]

Accepted: 17 November 2023 / Published online: 30 November 2023

Abstract

Purpose Skin fungal infections are widely spreading worldwide and are considered a main cause of skin, mucous membranes, and systemic diseases. In an approach to enhance the topical delivery of miconazole nitrate (MZN) as a poorly permeable antifungal agent, spanlastics nanocarriers as a type of elastic vesicles were adopted in the current work.

Methods MZN spanlastics were prepared and optimized according to a D-optimal response surface design to investigate the influence of formulation variables, edge activator (EA) percentage, EA type on particle size (PS), and drug entrapment efficiency percentage (% EE) as dependent variables. The spanlastics optimized formula (F7) was further assessed for its elasticity and physico-pharmaceutical properties before being incorporated into a gel. The F7 gel formula was also examined for its physical properties, in vitro release, in vitro antifungal activity against *Candida albicans* (ATCC® 10231), and ex vivo skin deposition studies. The results of the F7 gel formula were compared to the F7 aqueous dispersion.

Results The D-optimal design revealed that F7, developed using Tween 60 as EA and Span 60 at a weight ratio 2:8, is the optimized formula. F7 was an elastic, spherical, non-aggregated vesicle with an average PS of 210 nm and a drug entrapment efficiency of 90%. The drug was present in an amorphous form within the vesicles. The gel form of F7 showed a prolonged drug release behavior relative to the solution form, where 75% of the drug was released over 10 h for the former and 5 h for the latter. The antifungal study revealed a significant ($p < 0.05$) increase in the zone of inhibition of *Candida albicans* (ATCC® 10231) demonstrated by spanlastics compared to MZN suspension at the same concentration level. MZN suspension showed cytotoxic activity at a concentration of 20 µg/mL and above; the incorporation of the drug in spanlastics dispersion or gel form increased the cell viability percentage. The skin deposition studies showed that F7 deposition in the dermal layer, where deep skin infections occur, is 164-folds that of the plain drug.

Conclusions The results confirm the potential application of MZN-spanlastics to treat deeply seated skin fungal infections.

Keywords Skin · Fungal infections · *Candida albicans* · Miconazole nitrate · Spanlastics · D-Optimal design · Edge activator

Introduction

Although many fungi thrive in our daily lives without causing harm, the incidence of fungal infections appears to be rising worldwide. Fungi can cause skin and mucous membrane diseases and systemic infections of many internal organs. Skin or mucosal membrane fungal infections are the most common reason for victims to contact dermatologists. Cutaneous fungal infections affect 20–25% of the human population. Immunocompromised patients are at a high risk of infection, especially those who suffer from viral infections or use chemotherapeutic agents [1, 2].

Skin fungal infections may be classified according to the level of tissue invasion: superficial, cutaneous, or subcutaneous. When invading fungus affects only the outermost skin layers, the resulting infection is known as a superficial fungal infection. A superficial fungal infection raises the skin's pH, accompanied by inflammation and mild scaling at the infected site. In this situation, the skin's barrier function deteriorates [3–6].

✉ Omar A. Elkady
oalkady@msa.edu.eg; kady_omar@hotmail.com

[1] Department of Pharmaceutics and Industrial Pharmacy, Faculty of Pharmacy, October University for Modern Sciences and Arts (MSA), Giza 12451, Egypt

[2] Department of Microbiology and Immunology, Faculty of Pharmacy, October University for Modern Sciences and Arts (MSA), Giza 12451, Egypt

Cutaneous fungal infection, or dermatomycoses, occurs when the invasion reaches the epidermal layer with or without skin appendages such as nails and hairs. A cellular immunological response may be triggered as a result of the infection, causing pathological changes in individuals. Furthermore, the infection can spread to the dermal or subcutaneous regions, resulting in a subcutaneous fungal infection, e.g., *Candida albicans*. In this case, the infected areas are characterized by ulceration or infiltrating nodular lesions [7–9].

Azole-based antifungal drugs can reduce fungal properties by inhibiting cytochrome P450, responsible for the 14-alpha-demethylation pathway. The medication works well for pityriasis versicolor, tinea, otomycosis, and vulvovaginal candidiasis. According to the biopharmaceutics classification system, miconazole (MZN) is a class II drug. MZN is characterized by poor water solubility with a water partition value of around 6.25 in octanol, and limited skin penetration is observed for the drug [10].

Traditionally, skin fungal infections are treated using conventional topical dosage forms, e.g., lotions, creams, and gels containing antifungal drugs [11]. Nanocarriers have been employed to overcome the drug's poor permeability, maintain and control medication release, ensure direct contact with the stratum corneum, and shield the drug against chemical or physical instability [11]. The aforementioned benefits, in turn, reduce negative effects and dose frequency. Several nano-based formulation techniques have been previously investigated to enhance MZN skin penetration [3, 10, 11]. Miconazole nitrate has been loaded in solid lipid nanoparticles [12, 13], nanostructured lipid carriers[14], chitosan nanoparticles [15], transferosomes [16], ultra-flexible liposomes [17], propylene glycol nanoliposomes [18], cubosomes [19], nanoemulgel [20], nanoemulsion [21], and as an inclusion complex in β cyclodextrin [22].

Spanlastics are a type of elastic vesicles. It is composed of a non-ionic surfactant and an edge activator. Nonionic surfactants have low toxicity and compatibility with biological systems [23]. The non-ionic surfactant Span 60 has saturated alkyl chains and a lipophilic character. This amphiphilic property of the Span 60 allows the formation of unilamellar or multilamellar matrix vesicles. The surface-active features of this surfactant would enhance the edge activator's activity, resulting in a decrease in interfacial tension and the consequent formation of fine spanlastics dispersion [24].

On the other hand, the edge activators belong to a unique class of hydrophilic surfactants owing to their high HLB values. They are also considered single-chain surfactants that reduce the interfacial tension of the vesicles, destabilize them, and make the bilayer vesicles more deformable. Hence, they provide these vesicles' lipid bilayer membranes with flexibility and production systems with varying degrees of packing disruption. Vesicles improve drug permeability by expanding the biological membranes' pore size momentarily. This mechanism, in turn, allows larger vesicles to fit and permeate the skin [24–26].

The preparation and optimization of the nanovesicles can be facilitated by utilizing computer-aided designs. For this reason, optimal designs were utilized being computer-aided rather than orthogonal, like traditional response surface methodology (RSM) types. In these designs, the impacts of the variables are associated. The key advantage in this case is that it may be used to fit any model (first and second orders, quadratic, or cubic) or for any specific research goal, such as screening or generating a response surface. Furthermore, optimal designs allow fewer experimental trials than traditional types and have a limited design space. Based on the number of trials, the *R*-square values, and the fitted models of Akaike and Bayesian information criteria, determined that the D-optimal design is the best design for generating response surfaces. These findings were supported by Ranade and Thiagarajan's 2017 statistical comparison of several RSM designs [27]. The D-optimal design provides several equations to aid in the identification of the optimum formula. The selection of the optimum formula is based on employing a variety of variables that can be studied to correlate their effect on various responses: drug entrapment efficiency, absolute zeta potential value, in vitro drug release, particle size, and polydispersity index [28–30].

In the current study, miconazole nitrate was selected as a model antifungal drug for the treatment of deeply seated skin fungal infections. The drug was incorporated into spanlastics to enhance drug permeation into the deeper skin layer. A D-optimal design was employed to produce the least number of formulas that can be prepared to study the effect of surfactant level (at three levels) and EA type (at six levels) as independent variables on the responses, namely particle size and % EE of the drug.

Materials and Methods

Materials

Miconazole nitrate (MZN) was kindly supplied by Medical Union Pharmaceuticals, Egypt. Brij 35, Brij 58, Brij 97, and dialysis cellulose membrane (cut-off 14,000 g/mol) were purchased from Sigma-Aldrich, USA. Acros Organics, USA, supplied Span 60, Tween 20, Tween 60, and Tween 80. Propylene glycol 4000 was obtained from Loba-Chemie, India. Triethanolamine and ethanol were purchased from ADWIC, Egypt. Carbopol 934 was acquired from Goodrich Chemical Company, USA. The buffer constituents were obtained from El-Nasr Pharmaceutical Chemicals Co., Egypt: disodium hydrogen phosphate and potassium dihydrogen phosphate. All other solvents and chemicals were of analytical grade and were purchased and used as received.

Methods

Preparation of Miconazole Nitrate-Loaded Spanlastics Using D-Optimal Design

The composition of the various MZN-loaded spanlastics is listed in Table 1. The materials used in preparing the spanlastics are considered safe (GRAS), besides being FDA-approved [31]. Span 60, a non-ionic surfactant (SAA), was selected as the membrane-forming material. In addition, a range of non-ionic SAAs with various HLB values were employed as edge activators (EAs). Generally, the non-ionic surfactant class was selected owing to its safety, compatibility, and stability relative to the other surfactant classes [31].

Due to its simplicity and reproducibility, the ethanol injection method was adopted to prepare MZN-spanlastics [32, 33]. MZN (0.2 g) and the surfactant Span 60 were dissolved in 3 mL of 100% ethanol. The ethanolic solution was gently injected into a warmed aqueous medium containing the EA and constantly stirred on a magnetic stirrer (Jenway 1000, Jenway, UK) for 30 min until spanlastics dispersion (10 mL) was formed. The temperature was set to 80 °C and the stirring speed to 1000 rpm. The total SAA percentage in the formula (Span 60 and EA) was kept constant at 2% (w/v) of the total formulation volume (10 mL). In addition, the Span 60 percentage was varied in relevance to the EA percentage so that their sum would make 100% of the total SAA percentage used in the formula. To ensure that all of the alcohol was removed, the dispersion was stirred for another hour at the same room temperature and speed. The prepared formulas were left to mature overnight and then stored at 4 °C for further studies [34].

Experimental Design MZN-loaded spanlastics were prepared as proposed by D-optimal design using Design-Expert® 12.0.3.0 software (Stat-Ease Inc., USA) to examine the influence of formulation variables on the vesicle properties. In this design, two independent factors were evaluated, namely the percentage of edge activator (EA) (*A*) and the type of EA (*B*). The dependent variables were particle size (PS) (*R*1) and % EE (*R*2). The first independent factor was studied at 2 levels (10 and 30%) and 1 center point (20%), whereas the second was studied at 6 levels, namely Brij 35, Brij 58, Brij 97, Tween 20, Tween 60, and Tween 80, where 17 possible combinations were experimented as shown in Table 1 [35]. A summary of the factors and their levels is presented in the supplementary material, Table S1.

Model Selection and Validation The best-fitted models for both *R*1 and *R*2 were selected based on the lowest model *p*-value (significant), highest R^2 value, highest lack of fit *p*-value (non-significant), and where the difference between the predicted R^2 and the adjusted R^2 is in reasonable agreement (less than 0.2) [36, 37].

Optimized Formula Selection and Evaluation Based on the desirability approach, numerical optimization was carried out by selecting PS between 150 and 250 nm and maximizing the % EE. All factor weights were equal and set to ½. [38] The optimized formula, proposed by the software was prepared in triplicate and assessed by re-measuring the dependent variables and comparing them with the expected results, yielding the percentage bias; consequently, the validity of the design was checked. The

Table 1 Composition of the various formulas of MZN-loaded spanlastics and the responses measured. Data express the mean ± range, where $n = 3$

Formula code	EA (%)	Type of EA	*R*1 (particle size (nm))	*R*2 (entrapment efficiency (%))
F1	10	Brij 97	201 ± 6.03	80 ± 3.2
F2	10	Tween 80	170 ± 5.1	78 ± 3.12
F3	30	Tween 20	410 ± 12.3	30 ± 1.2
F4	10	Brij 35	338 ± 10.14	55 ± 2.2
F5	30	Brij 58	200 ± 6	58 ± 3.16
F6	30	Tween 60	90 ± 2.7	85 ± 3.4
F7	20	Tween 60	210 ± 0.28	90 ± 3.6
F8	30	Brij 35	207 ± 6.2	40 ± 1.6
F9	30	Brij 97	108 ± 4.86	70 ± 2.8
F10	10	Tween 80	170 ± 5.1	78 ± 3.12
F11	30	Tween 60	90 ± 2.7	82 ± 3.4
F12	10	Brij 58	302 ± 9.06	68 ± 2.72
F13	30	Brij 58	203 ± 6.8	58 ± 3.16
F14	10	Tween 20	730 ± 21.9	50 ± 2
F15	10	Brij 35	338 ± 14.8	55 ± 2.2
F16	30	Brij 97	108 ± 4.86	70 ± 2.8
F17	30	Tween 80	105 ± 4.71	68 ± 2.72

optimized formula was subjected to further investigations such as drug released percentage, physico-pharmaceutical characterization, and an *ex vivo* skin deposition test. For some tests, an adequate volume of the prepared aqueous dispersion was lyophilized to obtain it in powder form. The F7 aqueous dispersion was transferred to a 15-mL falcon tube and frozen overnight at −20 °C. After that, the sample was lyophilized using a Novalyphe-NL 500 freeze-dryer (Savant Instruments Corp., USA) for 24 h under a pressure of 7×10^{-2} mbar at −45 °C. The fluffy powder obtained was then kept in a dry, cool place for further use.

Statistical Analysis Statistical analysis was performed using Design-Expert® 12.0.3.0 software. Data was analyzed using one-way analysis of variance (ANOVA), and differences were considered significant when p was less than 0.05.

Characterization of Miconazole Nitrate-Loaded Spanlastics

Particle Size, Polydispersity Index, and Zeta Potential Measurements Dynamic light scattering was utilized to determine the average particle size (PS) and polydispersity index (PDI) of the developed particles at 25 °C using a Malvern Zetasizer (Nano-ZS, Malvern Instruments, Malvern, UK). Before measuring the PS, all formulations were adequately diluted with distilled water to guarantee a proper scattering intensity [39, 40]. The PDI was employed to indicate the homogeneity of the formulas, where a small value implies a homogenously sized vesicle and vice versa. The measurement was conducted three times for each sample, and the mean ± SD was calculated.

The vesicles' zeta potential (ZP) was assessed using the same instrument by detecting their electrophoretic mobility in an applied electrical field. The ZP measurements were determined in double-distilled water. Three replicates for each formula were taken [39, 41]. The ZP indicates the physical stability of the prepared particles, where a value above +30 mV or below −30 mV suggests the stability of the particles.

Entrapment Efficiency To determine the amount of MZN entrapped in the formulas, the MZN-loaded vesicles were centrifuged at a rotation speed of 15,000 rpm and a temperature of 4 °C for 1 h (Laborzentrifugen, 2k15, Sigma, Germany). The supernatant was then separated from the particles, and the amount of the free drug was measured spectrophotometrically at λmax 271 nm (Shimadzu UV spectrophotometer, 2401/PC, Japan). The entrapped percentage (EE%) of the drug was then calculated from Eq. 1 [41]:

$$\mathrm{EE}\ (\%) = \frac{D_t - D_u}{D_t} \times 100 \quad (1)$$

where D_t is the total amount of drug, and D_u is the amount of entrapped drug [42, 43].

Elasticity Measurement The extrusion technique Van den Bergh et al. [44] described was followed to assess the elasticity of the optimum formula for spanlastics aqueous dispersion (F7). F7 was diluted and extruded through a 220-nm pore-size microporous filter (Jinteng Experiment Equipment Co., Ltd., China) under a constant pressure of 2.5 bar (Haug Kompressoren AG; Büchi Labortechnik AG, Flawil, Switzerland). The particle size was compared before and after extrusion, and the percentage of deformation was calculated [45].

Physico-pharmaceutical Characterization of the Optimized Formula

Transmission Electron Microscopy (TEM) The morphological examination of the optimized MZN spanlastics formula was carried out using a transmission electron microscope (JEM-2100, Jeol, Japan) at an acceleration voltage of 80 kV. The vesicles were properly diluted, and one drop was applied to a carbon-coated copper grid surface and dehydrated. Phosphotungestic acid, at a concentration of 2%, was used to stain the sample, which was dehydrated again at ambient temperature to give a good contrast upon TEM inspection [41].

Differential Scanning Calorimetry (DSC) The thermograms of pure MZN powder and lyophilized F7 (the optimized MZN-spanlastics formula) were studied using a differential scanning calorimeter (DSC-50, Kyoto, Japan). An amount of 2 mg of each sample was loaded in aluminum pots, and the temperature was raised gradually at a rate of 10 °C/min from 25 to 300 °C under an inert nitrogen flow of 25 mL/min [41, 46].

Incorporation of MZN and Optimized Formula F7 in Carbopol Gel

Preparation of Carbopol Gel A Carbopol gel was formulated to incorporate the F7 and free medication within it. A quantity of 2 g of Carbopol 934 was dispersed in distilled water using a magnetic stirrer operating at 800 rpm for 60 min. The addition of propylene glycol 4000 (20 g) was carried out incrementally to the mixture. The addition of triethanolamine was carried out in a dropwise manner to achieve neutralization of the mixture. Manual stirring was performed using a glass rod until gelation occurred, and the resulting solution's pH was measured [47].

Incorporation of Free MZN and Optimized MZN-Spanlastics in Gel The prepared gel was used as a vehicle for the free drug and optimized formula, where an amount of 0.6 g of the drug was added to 15 g of the gel, and the weight was completed to 30 g with distilled water. Therefore, the MZN percentage in the gel was 2%.

Similarly, the optimized MZN-spanlastics in an amount equivalent to 0.6 g of the free drug was incorporated into the gel, and likewise, the MZN percentage in the spanlastics gel was 2% [41].

Characterization of Gel Formulas

Visual Inspection The prepared gel formulations' color, homogeneity, consistency, and spreadability were visually inspected [47, 48].

pH To determine the pH of the formula, a sample of the produced gel weighing 1 g was weighed and completed to 10 g with distilled water. The pH of the diluted sample was measured using a Jenway pH-Meter (model 3510, UK) [47, 48].

Viscosity The viscosity of the prepared gels was measured using a Brookfield rheometer with a spindle CP 41. The viscosity test was performed at room temperature with a rotating speed of 1 rpm [47, 48].

Drug Content An amount of 100 mg of the gel formulations was dissolved in 20 mL of ethanol and filtered, and the volume was completed with 10 mL of distilled water in a volumetric flask. The drug concentration in the solution was detected spectrophotometrically at 271 nm [47].

In Vitro Drug Release Studies of the Optimized Formulas in Aqueous Dispersion and Gel Form

The in vitro drug release profiles were performed using the membrane diffusion method for the following samples: the optimized MZN-spanlastics aqueous dispersion formula (F7), MZN-spanlastics gel (F7 gel), MZN gel, and MZN aqueous suspension. Before commencing the experiment, the cellulose membrane was soaked in a phosphate-buffered saline solution (pH = 5.4) for 24 h at room temperature. Afterward, 1 mL of each sample (or an amount equivalent to 20 mg of the drug) was loaded into the cellulose membrane, and both ends of the membrane were tightly tied. The loaded membrane was dropped into a beaker containing 300 mL of a phosphate-buffered saline solution with a pH of 5.4. The beaker was covered with parafilm and placed in an incubator shaker (IKA KS 4000, Germany). The shaker operation speed was 50 rpm, and the temperature was 37 ± 0.5 °C. At specific time intervals, aliquots of 5 mL were withdrawn and substituted by an equivalent volume of fresh buffer solution to maintain a constant volume. The withdrawn samples were analyzed spectrophotometrically at λmax of 271 nm to determine the percentage of the released drug. The results are presented as mean values ± SD of the percentage of drug release as a function of time for a total of three repeats per experiment [34]. The release data were fitted to various release kinetic models: zero, first, Higuchi diffusion, Hixson-Crowell, and Korsmeyer-Peppas models.

In Vitro Antifungal Activity Study of the Optimized Formulas in Aqueous Dispersion and Gel Form

In Vitro Antifungal Activity by Well Diffusion Assay The in vitro antifungal assay was used to determine and compare the samples' antifungal properties against *C. albicans* (ATCC® 10231). The tested samples were MZN suspension, MZN gel, the optimized MZN-loaded spanlastics (F7) aqueous dispersion, and F7 incorporated in the gel. The yeasts from a 24-h culture on Sabouraud dextrose agar (SDA) were subcultured to create the inoculum. The culture was left in the incubator overnight; afterwards, 5–6 colonies of the organism were transferred to 0.9% saline, and the suspension turbidity was adjusted to match the 0.5 McFarland standard (9.95 mL of 1% sulfuric acid (H_2SO_4)) according to the Clinical and Laboratory Standards Institute (CLSI) protocol. A fresh SDA medium was prepared according to the manufacturer's recommendation and poured into plates at a depth of 5 to 6 mm, and the plates were left to air dry for 30 min. The adjusted culture in saline was swabbed on the prepared SDA plates in three different directions to ensure complete coverage of the agar surface. The antifungal assay was done using both well and surface agar assays. As for the well agar assay, four wells, each 4 mm in diameter, were cut out of the agar using a sterile cork borer, and 100 µL of the tested sample (20 mg/mL) was placed into each well.

On the other hand, in the surface agar assay, 10 µL of the tested antifungal agent was placed onto the agar surface and left to dry. Plates were incubated at 35 °C for 24 h. Zones of complete inhibition were measured in millimeters. The assay was repeated three times for confirmation [49, 50].

In Vitro Antifungal Activity by Broth Microdilution Method The minimum inhibitory concentration (MIC) was determined using the broth microdilution method for MZN-containing samples against *C. albicans* (ATCC® 10231), namely MZN suspension, MZN gel, F7 aqueous dispersion, and F7 gel [51]. The media utilized in this test was prepared, similar to the "In Vitro Antifungal Activity by Well Diffusion Assay" section; the cultures were incubated overnight, and their turbidity was adjusted with 9.95 mL of 1% sulfuric acid (H_2SO_4) to match a 0.5 McFarland standard. Finally, the media were further diluted to give a final concentration

equivalent to 10^6 CFU/mL according to the CLSI protocol. On the other hand, the stock solution of MZN-containing samples (20 mg/mL) was serially diluted using sterile Sabouraud dextrose broth (SDB) to concentrations between 0.48 and 500 µg/mL.

One hundred microliters of the adjusted bacterial culture were added to an equal volume of the diluted MZN samples in a 96-well microtiter plate. Two controls were utilized: a negative control (Sabouraud broth only) and a positive control (Sabouraud broth with *C. albicans*) to confirm medium sterility and organism viability, respectively. The plates were then incubated at 35 °C for 24 to 48 h. The effect of loading MZN into spanlastics and their gel formulations was determined by measuring the change in the MIC of pure MZN. This loaded formulation's synergistic or antagonistic activity was reflected by a decrease or increase in the MIC values, respectively, compared to MZN suspension.

The MIC was recorded as the highest dilution of the antifungal agent, which gave no visible growth. Breakpoints for *C. albicans* were set by CLSI for azoles as follows: itraconazole (susceptible, MIC < 1 µg/mL and resistant, MIC ≥ 1 µg/mL) and fluconazole (sensitive, MIC ≤ 2 µg/mL and resistant, MIC ≥ 8 µg/mL). There was no defined breakpoint for miconazole; however, previous research indicated that *Candida* sp. is susceptible and resistant at MIC ≤ 5 µg/mL and MIC > 5 µg/mL, respectively [52, 53]. The experiment was conducted in triplicate. The mean and the standard deviation were recorded.

In Vitro Cytotoxicity Studies of Optimized Formulas in Aqueous Dispersion and Gel Form

MTT [3-(4,5-dimethylthiazol-2-yl)-2,5-diphenyltetrazolium bromide] test was used to assess cell viability in human skin fibroblast (HSF) cell lines. First, HSF cells (passage 10) were seeded in 96-well plates at a density of 5000 cells/well in full Dulbecco's modified eagle (DMEM) media with 10% fetal bovine serum (FBS) and 100 g/mL penicillin and streptomycin for 24 h at 37 °C in a 5% CO_2 incubator. The cells were then treated with a range of concentrations of MZN suspension, F7 aqueous dispersion, and F7 gel for 24 h at 37 °C and 5% CO_2. A volume of 100 µL of MTT/DMEM mixture with a ratio of 1:9 was applied to each well and incubated at 37 °C for 4 h to allow metabolically active cells to generate formazan crystals. After removing the medium, 100 µL of solubilized agent (DMSO) was added, and the optical density was measured spectrophotometrically at a wavelength of 570 nm (OD570). The viable cell percentage is directly proportional to the OD570 [54].

Ex Vivo Study of Gel Containing MZN and MZN-Spanlastics: Skin Deposition Test

Male Sprague Dawley rats weighing 220–240 g were sacrificed, and the back skin was meticulously removed using electrical clippers in accordance with ethical guidelines. The protocols of the conducted study were all approved by the MSA research and ethics committee (application number PT15/Ec15/2020F). Using a scalpel, the subcutaneous fats and cartilage were separated from the skin, which was then cleaned with phosphate-buffered saline, wrapped in aluminum foil, and frozen until needed.

Before use, the rat skin was given an hour to soak in phosphate buffer (pH 5.5) and divided into the proper sizes. The skin deposition experiment was performed on a Franz diffusion cell apparatus (MicroettePlus™; Hanson Research, Chatsworth, USA). The stratum corneum side of the skin was mounted in open, two-chamber Franz-type diffusion cells that were filled with phosphate buffer saline, pH 5.5. A thermostatically controlled water bath was used to place the diffusion cells, resulting in a skin surface temperature of 37 °C.

A Teflon-coated magnetic bar was used for stirring in the receptor compartment, which was filled with 10 mL of buffer; the stirring speed was set to 200 rpm. The stratum corneum surface was then covered with 1 g of the optimized formula and plain MZN gel. Experiments were conducted in triplicates, and the results from each experiment were presented as an average.

Following the incubation period, skin samples were taken out and thoroughly cleaned thrice using phosphate buffer soaked to remove any formulations that might have remained. The skin was then separated into three layers: stratum corneum, dermis, and epidermis. The stratum corneum was separated using a tape-stripping technique, whereas a pair of forceps was used to separate the dermis from the epidermis. Absolute ethanol was used to extract any drug retained on each skin layer sonicated for 30 min. Then, the skin extracts were filtered using 0.47 µm Millipore filters and injected into the HPLC coupled with an ultraviolet detector (Model SPD-10 A; Shimadzu) to quantify the drug content at λmax of 220 nm. The used column was Inertsil ODS: 4.6 × 250mm, 3.5 µm, and a mixture of water and methanol with a ratio of 15:85 was utilized as the mobile phase. The sample flow rate and temperature were set to 0.8 mL/min and 25 °C, respectively [41, 55, 56].

Stability Studies of Spanlastics Aqueous Dispersion

The change of the particle size as a function of time determines the formula's stability. Thus, the optimized formula was kept in the refrigerator for 6 months, and the particle

size and drug entrapment efficiency were re-measured and compared to the freshly prepared samples [57].

Results and Discussion

In this work, nanovesicles enriched with Span 60 as the chief constituent of the vesicular bilayer were prepared with a range of EA types. These vesicular carriers were then assessed, and the optimized formula was selected. The optimum formula was further tested for its capability to increase the cutaneous delivery of MZN to treat deep skin infections. To this objective, the nano-vesicular systems were developed using six types of hydrophilic EA: Tween 20, Tween 60, Tween 80, Brij 35, Brij 58, and Brij 97. In addition, the percentage of EA in the vesicular carrier was varied in correlation with the Span 60 percentages, to be 10, 90; 20, 80; and 30, 70%. The variables *A* (EA%) and *B* (type of EA), as well as the measured responses *R*1 (particle size (nm)) and *R*2 (entrapment efficiency (%)), are presented in Table 1.

D-Optimal Design Analysis

The measured responses of the 17 experimental runs (F1–F17) are shown in Table 1.

The Effect of Formulation Variables on the Particle Size (PS) of MZN-Loaded Spanlastics

The particle size is crucial in the formulation of cutaneous delivery systems as it affects the permeation capability of the carrier. Deeper skin permeation is guaranteed for vesicles with a diameter of less than or equal to 300 nm. However, as the vesicle diameter approaches 70 nm or less, the possibility of transdermal delivery increases. Therefore, in this study, a size range between 200 and 250 nm was targeted [58].

The prepared formulas PS (*R*1) ranged from 90 ± 1.2 to 730 ± 17.01 nm (Table 1). The effect of the two independent variables on the PS of MZN-loaded spanlastics is shown in Fig. 1A and B. The PDI of the vesicles ranged from 0.211 ± 0.10 to 0.366 ± 0.14. In addition, the ZP of all the formulations ranged from −22.9 ± 0.02 to −34.5 ± 0.31, indicating considerable stability of the particles [31] (data provided in the supplementary material; Table S2). PS was best fitted to a two-factor interaction (2FI) model showing the highest R^2 (Table 2). The interaction term AB shows how the response changes when the two variables simultaneously change at each level.

The ANOVA results revealed that the formula particle size is significantly affected by the level of EA (%) and its type ($p < 0.0001$). ANOVA results and fit statistics are summarized in Table 2. The PS was significantly affected by the level of EA, where a smaller particle size was observed for the high percentage of EA and vice versa (Fig. 1A) [35]. The reduction in the interfacial tension may explain the reduction in the particle size; hence, the emulsification power was increased [59]. At low EA %, the spanlastics surface may not be fully covered with the EA, leading to particle aggregation. The aggregates possess a lower surface area in an attempt to be fully coated with the present amount of EA. To sum up, larger vesicles are formed to increase the dispersion stability [60].

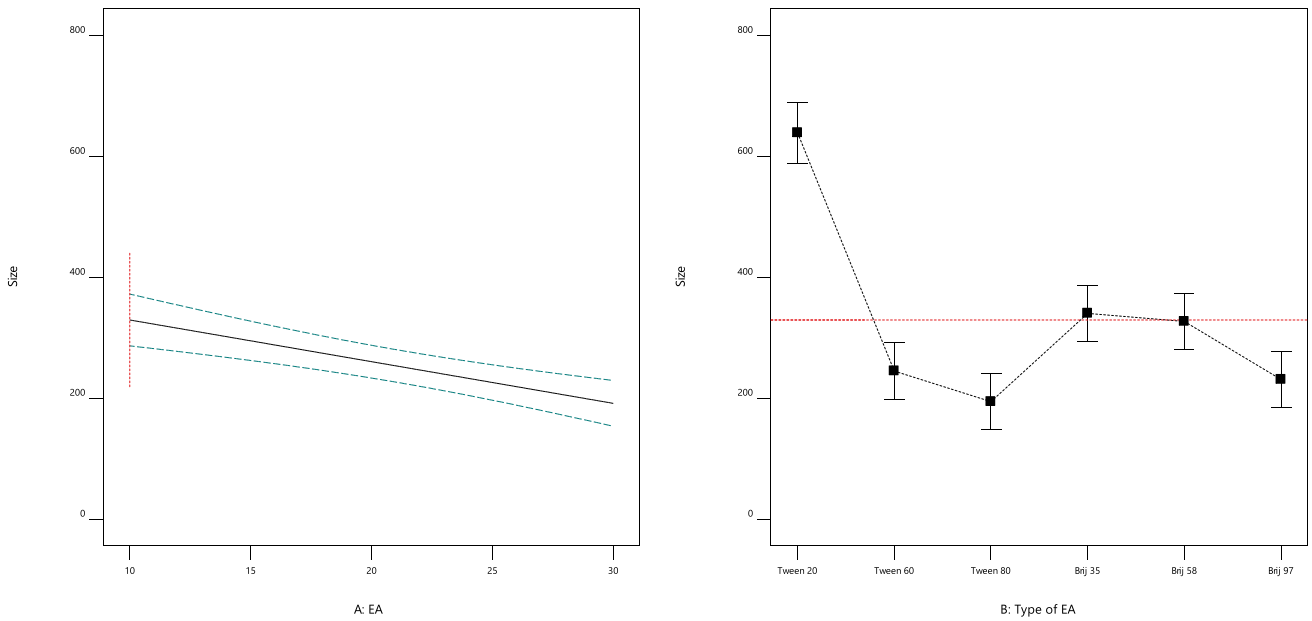

Fig. 1 The average effect of **A** EA % and **B** EA type on the size (nm) of the formed vesicles. Data express the mean ± SD, where $n = 3$

Table 2 Summary of ANOVA results and fit statistics for the D-optimal design studied responses (*R*1 and *R*2)

Response	Source	Sequential *p*-value	Lack of fit *p*-value	Adjusted R^2	Predicted R^2	
R1	Linear	**< 0.0001**	**< 0.0001**	**0.9047**	**0.7176**	Suggested
	2FI	**< 0.0001**		**1.0000**		Suggested
R2	Linear	**0.0005**	**0.8436**	**0.8020**	**0.6902**	Suggested
	2FI	0.8436		0.7132		

The bold values represent the values of the significant (suggested) models of the studied responses

Figure 1B correlates the particle size to the type of EA. The selected EAs had variable HLB values where the order of the HLB values for the used EAs from the lowest to the highest is Brij 97 < Tween 60 < Tween 80 < Brij 58 < Tween 20 < Brij 35. The use of EA with lower HLB (Tween 80, Brij 97, and Tween 60) (Fig. 1B) increases the vesicle hydrophobicity; as a result of the decreased water uptake and surface energy, smaller vesicles are formed [61].

The Effect of Formulation Variables on the Entrapment Efficiency of MZN-Loaded Spanlastics

The quantity of encapsulated MZN in spanlastics is critical for treatment efficiency. From Table 1, the % EE of the prepared vesicles ranged from 30 ± 0.12 to 90 ± 2.60%. The effect of the formulation variables on MZN % EE is illustrated in Fig. 2A and B. ANOVA results showed that MZN % EE is significantly affected by all studied factors ($p < 0.0001$ for all factors).

Figure 2A shows a direct correlation between decreasing the EA concentration and enhancing the drug entrapment efficiency in the formed vesicle. Increasing the concentration of the EA decreases the hydrophobicity of the formed vesicle due to the variation of the HLB value of Span 60 (HLB value = 4.7) and the used EA (HLB ranges 12.5–16.9). MZN is a lipophilic drug and thus might be better entrapped in the relatively lipophilic vesicles [14].

Figure 2B illustrates the effect of using various edge activators (EAs) on the entrapment efficiency of the formed vesicles. The highest entrapment efficiency has been observed for Tween 60, whereas Tween 20 showed the lowest entrapment efficiency. It may be concluded that two factors mainly affect the efficiency upon varying the type of edge activator. The first factor is the EA's HLB value; the lower the HLB value, the better the entrapment efficiency. Figure 2B illustrates that the highest entrapment efficiency value is observed for spanlastics prepared using EA, Tween 60 > Brij 97 > Tween 80.

Although the HLB value of Brij 97 is lower than Tween 60, the former showed a lower EE%. Therefore, another factor must have affected the entrapment efficiency, which is the unsaturation possessed by EA [62]. The more the unsaturation possessed by the EA, the more flexible the vesicle is formed due to the ability of the chain to bend. The elastic

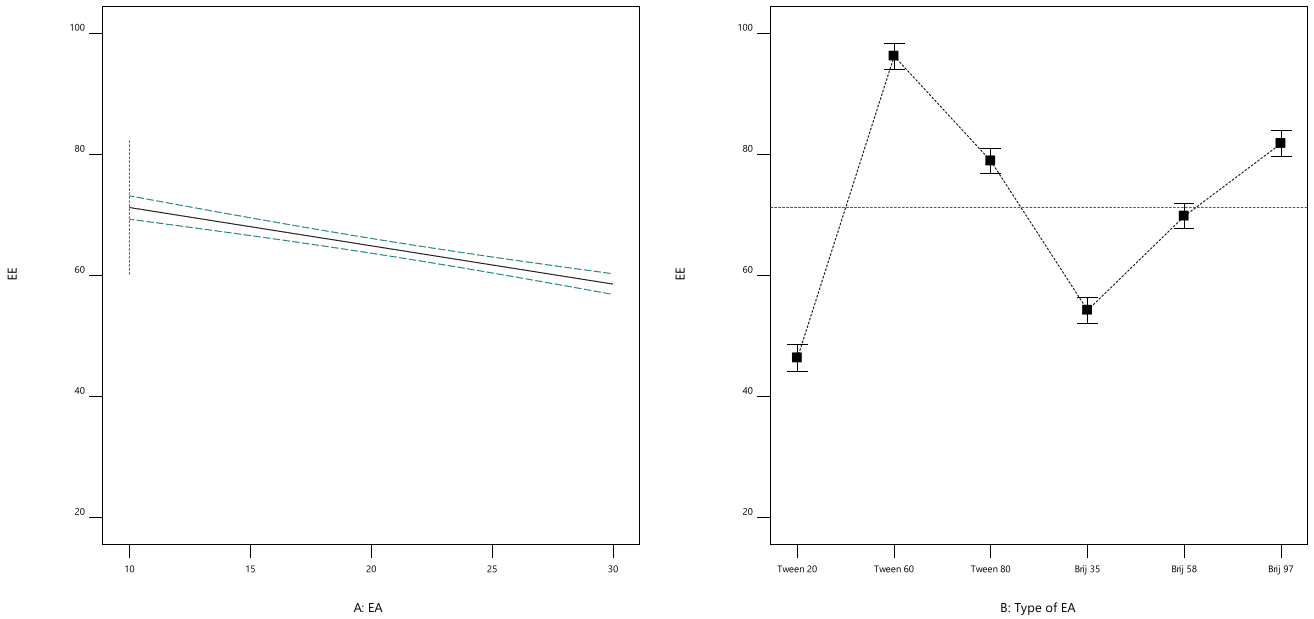

Fig. 2 The average effect of **A** EA % and **B** EA type on the drug entrapment efficiency (%) in the formed vesicles. Data express the mean ± SD, where $n = 3$

vesicles show a lower entrapment efficiency due to the drug's ability to escape from the formed vesicle. Considering this conclusion, using Tween 60 as EA exhibited a higher entrapment efficiency than the other surfactants due to forming rigid and hydrophobic vesicles relative to the other surfactants [60, 63].

Optimization Using D-Optimal Design

Formulation variables of MZN-loaded spanlastics were optimized for responses *R*1 (PS) and *R*2 (% EE). The target was to keep the PS between 200 and 250 nm and maximize % EE. The numerical optimization was performed using the Design-Expert software and yielded the optimal values of the variables depending on the selected desirability criteria. The highest desirability value (0.712) was found for the F7 formula; accordingly, it was chosen as the optimized formula. F7 was prepared in triplicate using Span 60 and 20% EA, namely Tween 60. F7 was prepared again, and its particle size and % EE were measured for the freshly prepared aqueous dispersion to be 210.5 ± 0.14 and 90.5 ± 1.54, respectively. The results of the freshly prepared sample were compared with those determined with the D-optimal design. The lower magnitude of errors (0.24 and 0.56%) observed for mean particle size and % EE, respectively, could indicate no marked differences and/or reasonable agreements between the previous and current experimental results. It is an index of robustness and high extrapolative ability of the generated optimization model [36]. Data verifying that the model can predict actual outcomes at the optimal settings determined from the analysis was added as supplementary material (Table S3).

Characterization of the MZN-Spanlastics Aqueous Dispersion Optimized Formula F7

The optimized formula F7 aqueous dispersion was subjected to elasticity and physico-pharmaceutical assessment. The MZN suspension and F7 aqueous dispersion were incorporated into a suitable gel base evaluated for visual inspection, viscosity, pH, in vitro release, and antifungal activity against *Candida albicans* (ATCC® 10231). Cytotoxicity studies were performed for MZN suspension to benchmark the cell viability percentage and compare it to F7 aqueous dispersion and F7 gel. Moreover, the MZN gel and F7 gel were used for the ex vivo skin deposition studies. Finally, stability studies were performed on F7 aqueous dispersion. The particle size and drug entrapment efficiency percentage were evaluated for the particles after six months of storage and compared to the freshly prepared formula values.

Elasticity Measurement

Elasticity testing of F7 revealed a minimal change (12%) in particle size pre- and post-extrusion, where the measured particle size was 210 and 185 nm, respectively. This deformability property allows the vesicles to spontaneously pass through biological membranes, reducing the chance of full vesicle rupture upon permeation. The incorporation of Tween 60 in the vesicle may account for the flexibility of the vesicle, as shown by the DSC studies. The shift of the Span 60's endothermic peak from 93, as stated in references [45], to 63.5 °C (presented in the supplemental section Fig. S2) may reflect the disruption in their packing characteristics. Thus, higher fluidity is observed for the vesicle. These results agree well with Badria and Mazyed's findings, which suggest that using EA has improved the elasticity of the prepared vesicles [38].

Physico-pharmaceutical Characterization of the Optimized Formula F7

Transmission Electron Microscopy (TEM) The TEM micrograph of formula F7 is illustrated in Fig. 3. Dark, almost spherical, non-aggregated particles were observed. The average particle size values observed from the TEM micrographs agree with those obtained from the Zetasizer measurement [41] [35].

Differential Scanning Calorimetry (DSC) Figure 4 represents the thermograms of MZN drug powder and lyophilized F7 formula. The DSC thermogram of pure MZN shows a melting endotherm at 186 °C, corresponding to its melting point [64]. The disappearance of the drug's endothermic peak in the lyophilized optimized formulation indicates the drug dispersion in an amorphous form [41].

Characterization of Gel-Containing MZN and Spanlastics Optimized Formula F7

Physical Property Studies

The prepared gel formulas were subjected to the evaluation tests illustrated in Table 3. The MZN gels were visually inspected, revealing an opaque, smooth, homogeneous gel with adequate spreadability. The measured pH was also appropriate for topical application. Similar observations were noted for the optimized spanlastics (F7) gel formula, except that the formula was transparent and had a higher viscosity than MZN-loaded gel [35].

In Vitro Drug Release of the Optimized Formulas in Aqueous Dispersion and Gel Form

Figure 5 shows the percentage of drug released through the cellulose membrane displayed as a function of time (*h*).

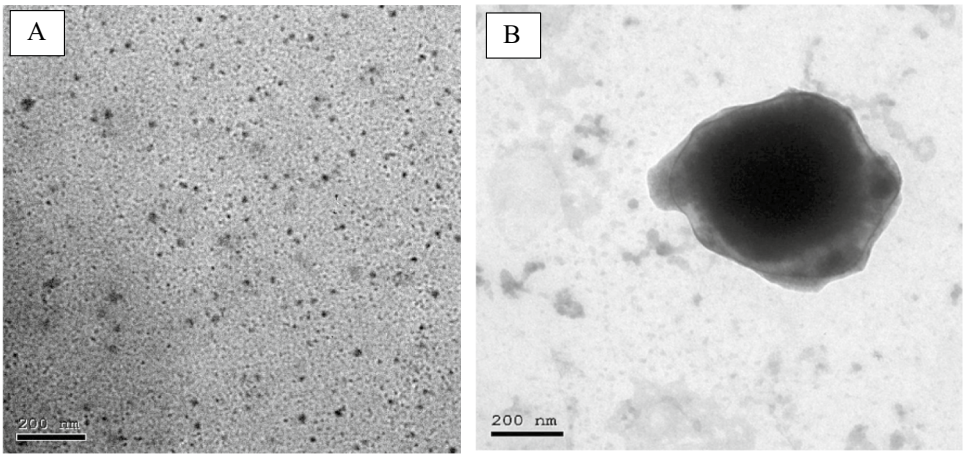

Fig. 3 TEM micrographs for the optimized formula of MZN loaded spanlastics F7. **A** Non-aggregated particles, and **B** almost spherical particles

Upon comparing the release profile of MZN from both the F7 and gel-loaded F7, a slower rate over a prolonged time was observed from the gel formula. In the case of F7, more than 70% of the drug was released within the first 6 h, while spanlastics gel showed a slower release rate, where only about 45% of the drug was released within the same period [35]. The MZN released percentage from the drug suspension and gel was 17 and 20% over 24 h, respectively. The aforementioned released percentages from the MZN formulas were significantly lower than the spanlastics formulas, owing to the poor water solubility of the drug.

The release data were fitted to various release kinetic models: zero-order, first-order, Higuchi diffusion, Hixson–Crowell, and Korsmeyer–Peppas models to determine MZN release behavior from the spanlastics gel. The coefficient of determination (R^2) was calculated for each fit model. The release data were best fitted to the Hixson-Crowell model based on the highest R^2 value of 0.9959, indicating that the main mechanism of drug release is based on the fact that there is a change in the surface area and diameter of the particle when there is dissolution, where there is a proportional relationship between the surface area of the particle and the cube root of its volume [65, 66]. Upon further fitting to the Korsmeyer-Peppas model, the diffusional exponent "n" was found to be between 0.43 and 0.85 ($n = 0.83$), indicative of anomalous (non-Fickian) transport where the rates of drug diffusion and polymer relaxation are comparable [36]. Generally, incorporating MZN in various nanoparticulate systems for topical delivery provides an extended-release profile. Al-Maghrabi et al. incorporated MZN in solid lipid nanoparticles, providing a controlled release profile for up to 48 h [13]. Similar findings were reported by Abdel-Rashid et al., where the drug release from polymeric nanocapsules and lipid nanocapsules was extended over 48 h. The reported findings agree well with our results; however, the spanlastics controlled the drug release over a shorter period, 24 h [54].

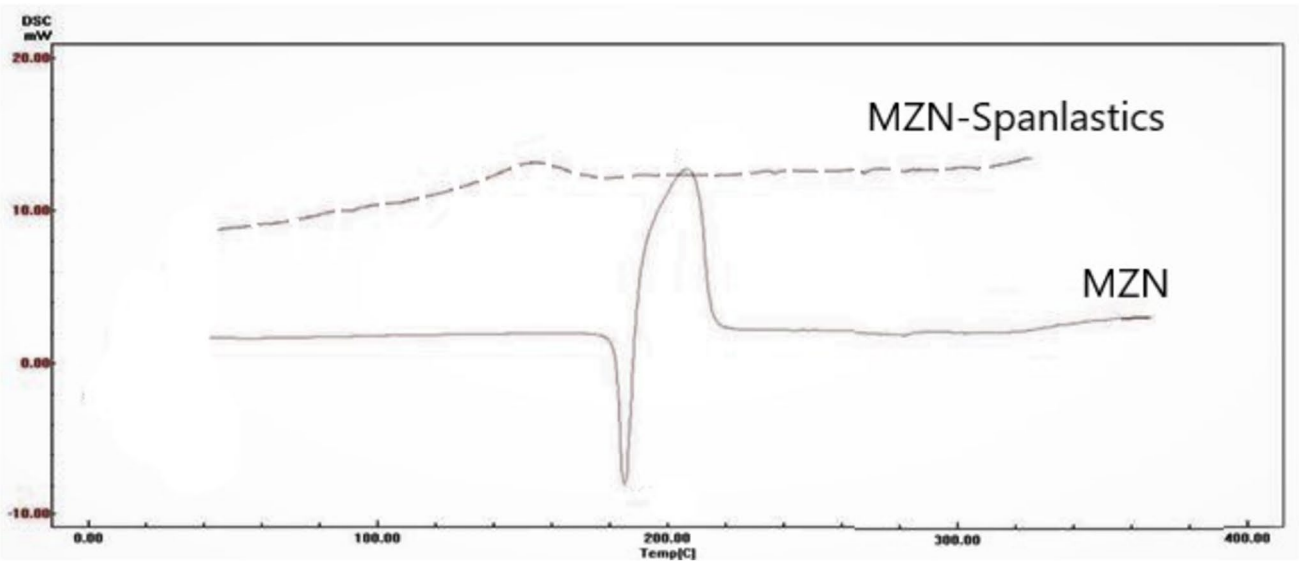

Fig. 4 DSC thermogram of pure MZN and lyophilized F7

Table 3 Physical properties of F7 optimized MZN-loaded spanlastics gel

Parameter	MZN gel	F7 gel
Clarity	Opaque	Transparent
Homogeneity	Homogenous	Homogenous
pH	5.5 ± 0.1	5.5 ± 0.1
Spreadability (cm)	2.5	2.3
Drug content	99.7 ± 0.2%	99.2 ± 0.25%
Viscosity (CP)	11,990	14,050

To conclude, incorporating the drug in the spanlastics enhanced the drug release profile due to the dispersion of the drug in an amorphous form within the nanovesicles, as proved by the DSC results.

In Vitro Antifungal Activity Study of the Optimized Formulas in Aqueous Dispersion and Gel Form

In Vitro Antifungal Activity by Well Diffusion Assay

Figure 6A shows the average value for the zone of inhibition diameter in mm for MZN suspension, MZN gel, F7 aqueous dispersion, and F7 gel on *Candida albicans* (ATCC® 10231) using well diffusion assay. The F7 dispersion and F7 gel showed an increase in the diameter of the fungal zone of inhibition and enhanced activity relative to MZN suspension and MZN gel preparation. Statistical analysis revealed a significant ($p < 0.05$) difference in inhibition zones of the F7 dispersion (31.0 ± 1.414 mm) and gel (29.0 ± 1.31 mm) form relative to MZN suspension (17.7 ± 0.707 mm) and gel (24.0 ± 1.414 mm). The highest zone of inhibition was reported for the F7 dispersion, ensuring that the drug incorporation in the nanovesicle enhanced its antifungal activity (Fig. 6B).

The agar overlay assay results were consistent with the well diffusion assay in Fig. 6B, where the F7 dispersion and F7 gel showed a wider zone of inhibition than MZN suspension and MZN gel. The pure gel did not show any antifungal activity against *C. albicans*. The F7 dispersion and F7 gel-enhanced antifungal effect may be attributed to the small size of particles formed in the presence of Tween 60, which results in a larger surface area and improved membrane permeability [67, 68].

Our findings agree with El-Meshad and Mohsen, where it was noted that itraconazole-loaded spanlastics showed more antimycotic activity against *C. albicans* than pure itraconazole. The enhanced antimycotic activity of itraconazole-loaded spanlastics was demonstrated by a higher zone of inhibition of the cultured *C. albicans* demonstrated by spanlastics compared to itraconazole powder at the same drug concentration [69]. In addition, Marques et al. reported that the spanlastics-loaded hydrogel formulation of luliconazole showed a greater zone of inhibition than the marketed formulation, providing optimum antifungal activity against *C. albicans* [70]. Finally, Shirland et al. reported that the niosomal gel of ketoconazole nitrate showed better antifungal activity due to its prolonged drug release [71].

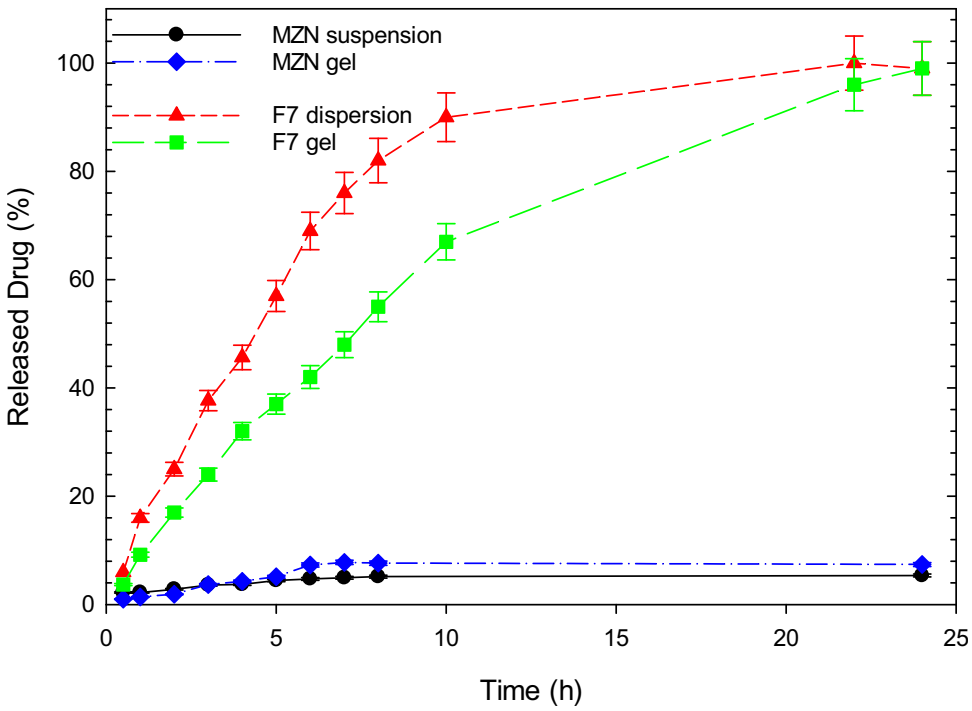

Fig. 5 In vitro drug release for (●) MZN aqueous suspension, (◊) MZN gel, (Δ) optimized MZN-spanlastics aqueous dispersion F7, and (□) optimized MZN-Spanlastics gel (F7 gel). Data are expressed as the mean ± SD, where $n = 3$

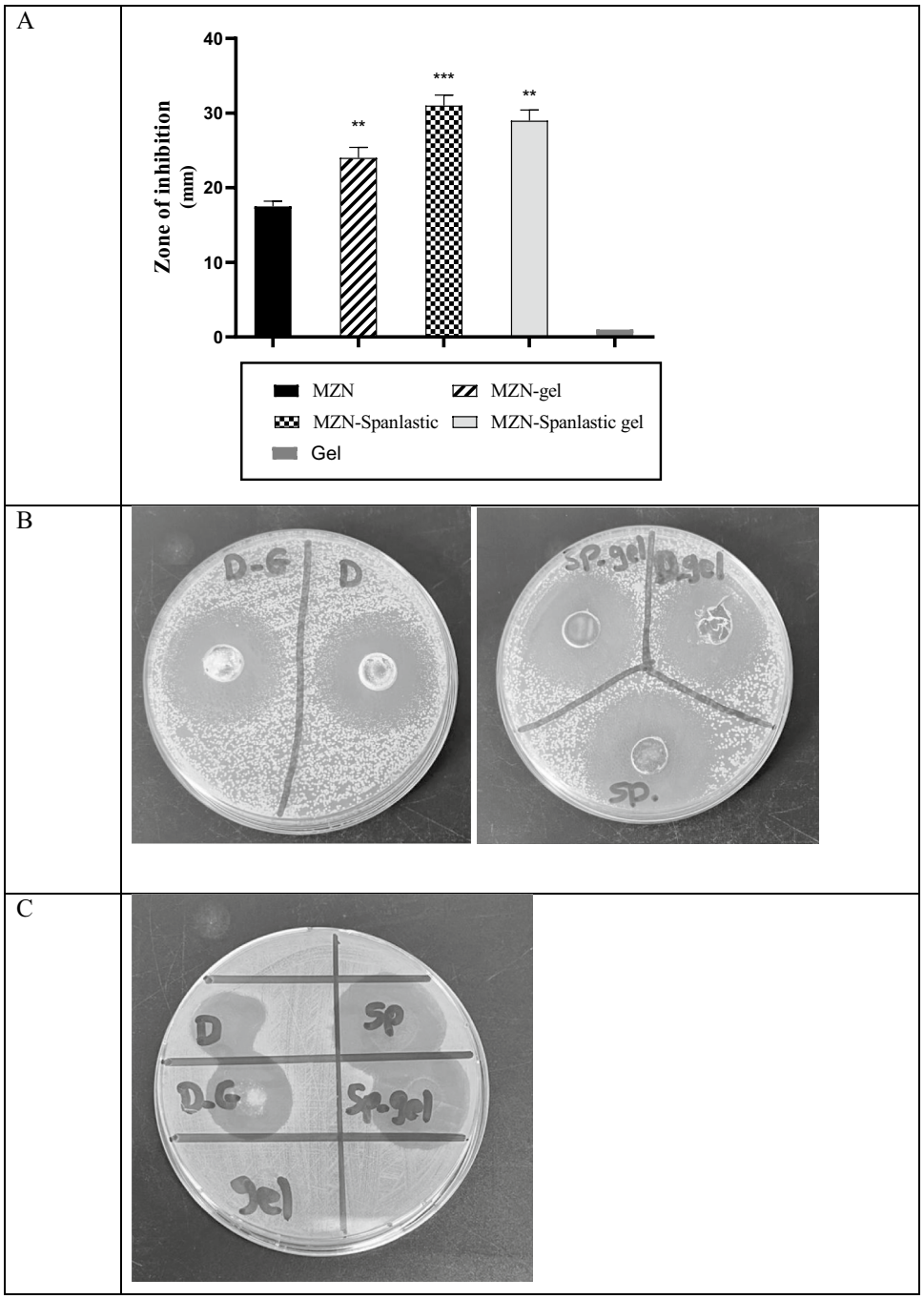

Fig. 6 The in vitro antifungal activity. **A** Bar chart showing the average zone of inhibition of different samples measured from well diffusion and agar overlay assay. The growth inhibition was measured in millimeters after incubation at 35 °C for 24 h. Data express the mean ± SD, where n = 3. Statistical analysis was done using Student's t test where statistical significance is represented by *p < 0.05, **p < 0.01, and ***p < 0.001. **B** Plates showing the zone of C. albicans (ATCC® 10231) using well diffusion assay, whereas **C** plate showing the zone of C. albicans (ATCC® 10231) using agar overlay assay. The symbols on the plate represent the following: D, MZN; D-G, MZN-gel; Sp, optimized MZN-spanlastics (F7) aqueous dispersion; Sp-gel, F7 gel; gel, gel alone

In Vitro Antifungal Activity by Broth Microdilution Method

The results of in vitro antifungal susceptibility profiles (MIC) of the tested antifungal against *C. albicans* (ATCC® 10231) are shown in Table 4. The MICs of pure MZN, MZN-gel, F7 dispersion, and F7 gel were detected against *C. albicans* (ATCC® 10231). *C. albicans* showed sensitivity to pure MZN, and its MIC was 0.96 µg/mL, as shown in Table 4. Loading MZN on the nanocarrier spanlastics reduced the MIC of MZN and increased the fungal sensitivity. As illustrated in Table 4, the MIC against *C. albicans* (ATCC® 10231) of F7 dispersion and gel formulas was reduced twofold relative to MZN suspension. The reduction in the MZN MIC for the spanlastics formulas may be related to the ability of spanlastics formulation to enhance the drug solubility, thus improving its penetration

Table 4 Results of antifungal MIC of pure MZN, MZN loaded with gel, MZN-loaded spanlastics, and MZN-Spanlastics gel formula against *C. albicans* (ATCC® 10231)

Fungal strain	Minimum inhibitory concentration (MIC)			
	MZN (µg/mL)	MZN-gel (µg/mL)	MZN-spanlastics (µg/mL)	MZN-spanlastics gel (µg/mL)
Candida albicans (ATCC® 10231)	0.96 ± 0.00 (S)*	3.84 ± 0.43 (S)	0.48 ± 0.00 (S)	0.48 ± 0.00 (S)

**S* sensitive

through the fungal cell wall and increasing its activity [72]. Incorporating the F7 dispersion into the gel subtly affected the MIC. On the other hand, the MZN gel MIC increased by fourfold relative to MZN suspension and eightfold relative to F7 formulas.

A study conducted by Marques et al. reported that a spanlastics-loaded hydrogel formulation of luliconazole showed no difference in the MIC values in comparison to the drug alone [70]. However, another study conducted by Aziz and co-workers demonstrated that tolnaftate-cosolvent spanlastics formulation enhanced the antifungal activity of tolnaftate, where the MIC of the spanlastics formula was reduced compared to the drug alone. The MIC reduction was correlated to the tolnaftate-enhanced solubility and, hence, better cell wall permeability [72].

In Vitro Cytotoxicity Studies of Optimized Formulas in Aqueous Dispersion and Gel Form

Figure 7 shows the human skin fibroblasts (HSF) cell viability percentage for a range of concentrations of F7 aqueous dispersion and F7 gel form compared to MZN suspension. The drug suspension showed a lower cell viability percentage relative to F7 aqueous dispersion and gel form, indicating the safety of the nanocarrier and the prepared gel. In general, MZN's cytotoxic impact can be attributed to the generation of ROS in human keratinocytes, which can cause oxidative stress and cell death. Furthermore, MZN is known to suppress cell proliferation by activating extrinsic and intrinsic apoptotic pathways [73, 74]. A published study corroborated our findings by demonstrating that the inclusion of MZN in polymeric and lipid nanocapsules resulted in an improvement in cell viability [54]

Ex Vivo Study of Gel-Containing Drug and Spanlastics: Skin Deposition Test

As the foremost objective of this study is the effective delivery of MZN to deeper skin tissues for the effective treatment of fungal infections, in vitro skin permeation and deposition behavior of MZN using a gel containing optimized spanlastics formulation (F7) in comparison to MZN-loaded gel were studied [75].

Rat skin was utilized for the in vitro skin deposition investigations due to its advantageous characteristics, including minimizing variation in drug permeability and ease of handling. While there exists a notable correlation between drug penetration rates in human and rat skin, it is often observed that the permeation rates of drugs in human skin are somewhat slower when compared to rats.

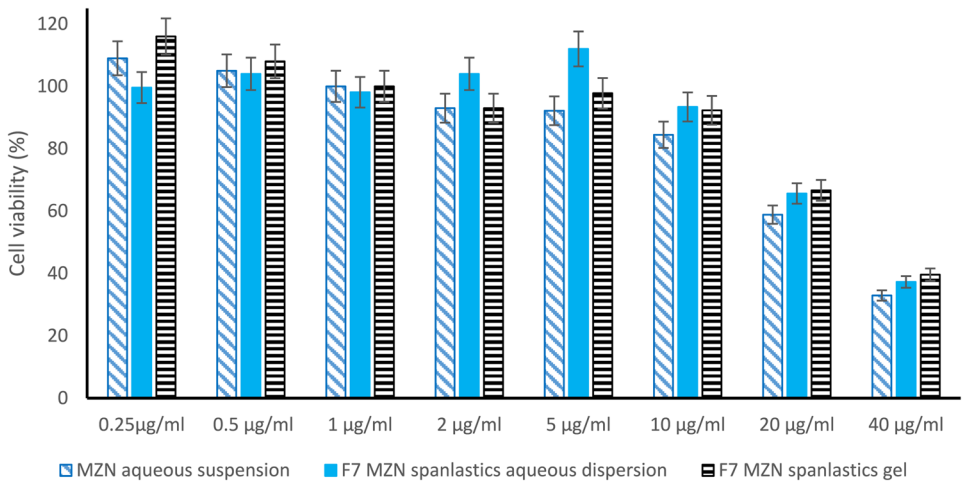

Fig. 7 Cell viability percentage for MZN aqueous suspension, F7 MZN-spanlastics optimized formula aqueous dispersion optimized formula, and F7 gel. Data express the mean ± SD, where n = 3

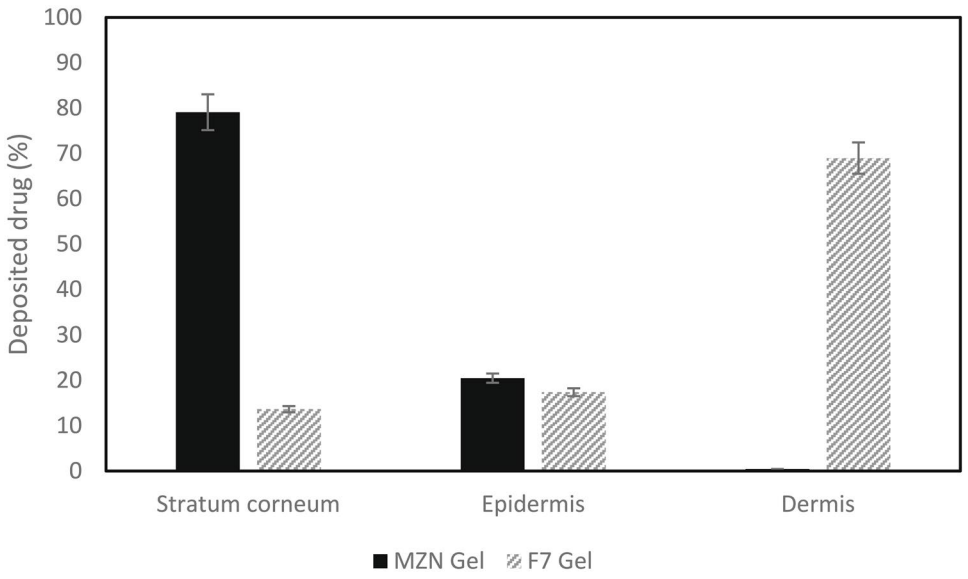

Fig. 8 Percentage of drug deposited in various skin layers for MZN gel and F7 gel. Data expresses the mean ± SD, where $n = 3$

The observed discrepancy can be ascribed to the comparatively larger thickness of human skin in comparison to that of rats [75].

Figure 8 depicts the deposition profiles of MZN, as measured 24 h after the commencement of the in vitro skin deposition analysis. The analysis utilized both the optimized MZN spanlastics–loaded (F7) gel and the MZN-loaded gel. The findings indicated that the F7 gel exhibited a greater percentage (70%) of drug deposition in the dermis compared to the epidermis and stratum corneum. In contrast, the proportion of the drug deposited in the stratum corneum was found to be 79%, surpassing the amounts deposited in both the epidermis and dermis for the MZN gel formulation. The deposition characteristics of F7 provide an overview of the efficacy of spanlastics as carriers for the treatment of cutaneous fungal diseases [75]. The enhanced deposition of the spanlastics formulas in deep skin tissues may be correlated to the vesicle's flexibility and particle size, which targeted deeper skin layers. Our findings are consistent with the study conducted by Shamma et al., which reported a twofold increase in retinoic acid skin deposition when incorporated into the spanlastics nanovesicles [41].

Stability Studies of Spanlastics Aqueous Dispersion

Upon comparing the results of the freshly prepared samples and the samples stored for 6 months, good stability was noted, indicated by no significant ($p > 0.05$) changes in the vesicle size or the drug % EE, as shown in Table 5.

Table 5 Effect of storage on properties of the optimum formulation F7

Parameter	Freshly prepared sample	After 6 months
PS	210.5 ± 0.14	220 ± 1.05
% EE	91 ± 1.54	90 ± 1.83

Conclusion

Miconazole nitrate–loaded spanlastics were successfully prepared and optimized using D-optimal response surface design for topical application targeting deeply seated skin fungal infection. Spanlastics formulated using 20% EA (Tween 60) and Span 60; F7 offered a good morphological characteristic in terms of size and polydispersity, vesicle elasticity, high drug EE% (90%), and a sustained drug release pattern. The physicochemical characterization revealed the presence of the drug in an amorphous form. The incorporation of F7 in a gel showed a slower release pattern relative to the solution form. Furthermore, F7 dispersion and gel formulas showed higher cell viability percentages and enhanced antimycotic action against *C. albicans* compared to MZN formulas. F7 gel was compared to MZN gel ex vivo skin deposition, where F7 gel showed a superior deposition in the dermal skin layer (70%) relative to the drug's (0.4%). To conclude, this formula carries great potential to be applied in treating deep skin fungal infections due to the mitigation of MZN downsides by enhancing its solubility and skin permeability.

Supplementary Information The online version contains supplementary material available at https://doi.org/10.1007/s12247-023-09800-y.

Author Contributions The authors contributed equally to this work and participated in the following: the conception or design of the work; the acquisition, analysis, or interpretation of data; drafting the work and revising it critically for important intellectual content; final approval of the version to be published; agreement to be accountable for all aspects

of the work in ensuring that questions related to the accuracy or integrity of any part of the work are appropriately investigated and resolved.

Funding Open access funding provided by The Science, Technology & Innovation Funding Authority (STDF) in cooperation with The Egyptian Knowledge Bank (EKB). There was no grant from any public, private, or non-profit funding body for this research.

Data Availability All data generated or analysed during this study are included in this published article [and its supplementary information files].

Declarations

Ethics Approval The protocol of the study was reviewed and approved by the Research Ethics Committee (application number PT15/Ec15/2020F) at the Faculty of Pharmacy, October University for Modern Sciences and Arts (MSA) (Giza, Egypt).

Conflict of Interest The authors declare no competing interests.

References

1. Ahmed S, Amin MM, Sayed S. A comprehensive review on recent nanosystems for enhancing antifungal activity of fenticonazole nitrate from different routes of administration. Drug Deliv. 2023;30(1):2179129.
2. Lockhart SR, Guarner J. Emerging and reemerging fungal infections. Semin Diagn Pathol. 2019;36(3):177–81.
3. Verma S, Utreja P. Vesicular nanocarrier based treatment of skin fungal infections: potential and emerging trends in nanoscale pharmacotherapy. Asian J Pharm Sci. 2019;14(2):117–29.
4. Zuber TJ, Baddam K. Superficial fungal infection of the skin. Where and how it appears, help determine therapy. Postgrad Med. 2001;109(1):117–32.
5. Gupta AK, Einarson TR, Summerbell RC, Shear NH. An overview of topical antifungal therapy in dermatomycoses. A North American perspective. Drugs. 1998;55(5):645–74.
6. Garg A, Sharma GS, Goyal AK, Ghosh G, Si SC, Rath G. Recent advances in topical carriers of antifungal agents. Heliyon. 2020;6(8):e04663.
7. Patel U, Chu J, Patel R, Meehan S. Subcutaneous dematiaceous fungal infection. Dermatol Online J. 2011;17(10):19.
8. Gretzula J, Penneys NS. Complex viral and fungal skin lesions of patients with acquired immunodeficiency syndrome. J Am Acad Dermatol. 1987;16(6):1151–4.
9. Noshi SH, Basha M, Awad GEA, Elmahdy Elsayyad NM. Miconazole nitrate loaded Soluplus®-Pluronic® nano-micelles as promising drug delivery systems for ocular fungal infections: in vitro and in vivo considerations. Research J Pharm and Tech. 2020;15(2):501–11.
10. Firooz A, Namdar R, Nafisi S, I. Maibach H. Nano-sized technologies for miconazole skin delivery. Curr Pharm Biotechnol. 2016;17(6):524–31.
11. Güngör S, Erdal MS, Aksu B. New formulation strategies in topical antifungal therapy. Journal of Cosmetics, Dermatological Sciences and Applications. 2013;03(1A):56–65.
12. Bhalekar MR, Pokharkar V, Madgulkar A, Patil N, Patil N. Preparation and evaluation of miconazole nitrate-loaded solid lipid nanoparticles for topical delivery. AAPS PharmSciTech. 2009;10(1):289–96.
13. Al-Maghrabi PM, Khafagy E-S, Ghorab MM, Gad S. Influence of formulation variables on miconazole nitrate–loaded lipid based nanocarrier for topical delivery. Colloids Surf B: Biointerfaces. 2020;193:111046.
14. Sanap GS, Mohanta GP. Design and evaluation of miconazole nitrate loaded nanostructured lipid carriers (NLC) for improving the antifungal therapy. J Appl Pharm Sci. 2013;3(01):46–54.
15. Jadhav K, Jadhav S, Sonawane D, Somvanshi D, Shah H, Patil P. Formulation and evaluation of miconazole nitrate loaded novel nanoparticle gel for topical delivery. J Pharm Res Int. 2021;33(44A):292–307.
16. Qushawy M, Nasr A, Abd-Alhaseeb M, Swidan S. Design, optimization and characterization of a transfersomal gel using miconazole nitrate for the treatment of candida skin infections. Pharmaceutics. 2018;10(1):26.
17. Pandit J, Garg M, Jain NK. Miconazole nitrate bearing ultraflexible liposomes for the treatment of fungal infection. J Liposome Res. 2014;24(2):163–9.
18. Elmoslemany RM, Abdallah OY, El-Khordagui LK, Khalafallah NM. Propylene glycol liposomes as a topical delivery system for miconazole nitrate: comparison with conventional liposomes. AAPS PharmSciTech. 2012;13(2):723–31.
19. Ka Khalifa M, Khalifa MK. Miconazole nitrate based cubosome hydrogels for topical application. Int J Drug Deliv. 2015;7(1):1–12.
20. Tayah DY, Eid AM. Development of miconazole nitrate nanoparticles loaded in nanoemulgel to improve its antifungal activity. SPJ. 2023;31(4):526–34.
21. Maha HL, Sinaga KR, Masfria. Formulation and evaluation of miconazole nitrate nanoemulsion and cream. Asian J Pharm. Clin Res. 2018;11(3):319–21.
22. Wang J, Cai Z. Investigation of inclusion complex of miconazole nitrate with β-cyclodextrin. Carbohydr Polym. 2008;72(2):255–60.
23. Alhakamy NA, Al-Rabia MW, Md S, Sirwi A, Khayat SS, Alotaibi SS, et al. Development and optimization of luliconazole spanlastics to augment the antifungal activity against candida albicans. Pharmaceutics. 2021;13(7):977.
24. Sharma A, Pahwa S, Bhati S, Kudeshia P. Spanlastics: a modern approach for nanovesicular drug delivery system. Int J Pharm Sci Res. 2020;11(3):1057–65.
25. Jacob L, Kr A. A review on surfactants as edge activators in ultradeformable vesicles for enhanced skin delivery. Int J Pharm Bio Sci. 2013;4(3):337–44.
26. El Zaafarany GM, Awad GAS, Holayel SM, Mortada ND. Role of edge activators and surface charge in developing ultradeformable vesicles with enhanced skin delivery. Int J Pharm. 2010;397(1-2):164–72.
27. Ranade SS, Thiagarajan P. Selection of a design for response surface. IOP Conf Ser Mater Sci Eng. 2017;263(2):022043.
28. Ahmed S, Kassem MA, Sayed S. Co-polymer mixed micelles enhanced transdermal transport of lornoxicam: in vitro characterization, and in vivo assessment of anti-inflammatory effect and antinociceptive activity. J Drug Deliv Sci Technol. 2021;62:102365.

29. Noshi SH, Dawoud MHS, Ibrahim M. A quality by design approach for the optimization of olmesartan medoxomil-orodispersible lyophilisates: In vitro/in vivo evaluation. J Appl Pharm Sci. 2022;12(6):172–85.
30. Ibrahim MS, Elmahdy elsayyad NM, Salama A, Noshi SH. Quality by design (QBD) as a tool for the optimization of indomethacin freeze-dried sublingual tablets: in vitro and in vivo evaluation. Int J App Pharm. 2021;13(5):160–71.
31. Kakkar S, Kaur IP. Spanlastics-a novel nanovesicular carrier system for ocular delivery. Int J Pharm. 2011;413(1-2):202–10.
32. Jaafar-Maalej C, Diab R, Andrieu V, Elaissari A, Fessi H. Ethanol injection method for hydrophilic and lipophilic drug-loaded liposome preparation. J Liposome Res. 2010;20:(3) 228–43.
33. Gaafar PME, Abdallah OY, Farid RM, Abdelkader H. Preparation, characterization and evaluation of novel elastic nano-sized niosomes (ethoniosomes) for ocular delivery of prednisolone. J Liposome Res. 2014;24:(3) 204–15.
34. Mazyed EA, Helal DA, Elkhoudary MM, Abd Elhameed AG, Yasser M. Formulation and optimization of nanospanlastics for improving the bioavailability of green tea epigallocatechin gallate. Pharmaceuticals. 2021;14(68):1–30.
35. Farghaly DA, Aboelwafa AA, Hamza MY, Mohamed MI. Topical delivery of fenoprofen calcium via elastic nano-vesicular spanlastics: optimization using experimental design and in vivo evaluation. AAPS PharmSciTech. 2017;18(8):2898–909.
36. Elkady OA, Tadros MI, El-laithy HM. QbD approach for novel crosslinker-free ionotropic gelation of risedronate sodium–chitosan nebulizable microspheres: optimization and characterization. AAPS PharmSciTech. 2020;21(1):14.
37. Manini G, Benali S, Raquez J-M, Goole J. Proof of concept of a predictive model of drug release from long-acting implants obtained by fused-deposition modeling. Int J Pharm. 2022;618:121663.
38. Badria F, Mazyed E. Formulation of nanospanlastics as a promising approach for improving the topical delivery of a natural leukotriene inhibitor (3-acetyl-11-keto-β-boswellic acid): statistical optimization, in vitro characterization, and ex vivo permeation study. Drug Des Devel Ther. 2020;2020(14):3697–721.
39. Griffiths PC, Cattoz B, Ibrahim MS, Anuonye JC. Probing the interaction of nanoparticles with mucin for drug delivery applications using dynamic light scattering. Eur J Pharm Biopharm. 2015;97: (part A):218–22.
40. Noshi SH, Ibrahim MS, Salama A, Fathy IA, Elsayyad NME. Chondroitin sulphate-chitosan polyelectrolyte complexes for etorocoxib transdermal delivery: in silico, in vitro and in vivo studies. Pharm Dev Technol. 2023;28(8):785–98.
41. Shamma RN, Sayed S, Sabry NA, El-Samanoudy SI. Enhanced skin targeting of retinoic acid spanlastics: in vitro characterization and clinical evaluation in acne patients. J Liposome Res. 2019;29(3):283–90.
42. Aljuffali IA, Pan TL, Sung CT, Chang SH, Fang JY. Anti-PDGF receptor β antibody-conjugated squarticles loaded with minoxidil for alopecia treatment by targeting hair follicles and dermal papilla cells. Nanomed. 2015;11:(6):1321–30.
43. Kharwade RS, Mahajan NM. Formulation and evaluation of nanostructured lipid carriers based anti-inflammatory gel for topical drug delivery system. Asian J Pharm. Clin Res. 2019;12(4):286–91.
44. Van den Bergh BAI, Bouwstra JA, Junginger HE, Wertz PW. Elasticity of vesicles affects hairless mouse skin structure and permeability. JCR. 1999;62(3):367–79.
45. Abdelbari MA, El-mancy SS, Elshafeey AH, Abdelbary AA. Implementing spanlastics for improving the ocular delivery of clotrimazole: in vitro characterization, ex vivo permeability, microbiological assessment and in vivo safety study. Int J Nanomedicine. 2021;16:6249–61.
46. Ibrahim MS, Elsayyad NME, Salama A, Noshi SH. Utilization of response surface design for development and optimization of rosuvastatin calcium loaded nano-squarticles for hair growth stimulating VEGF and IGF production: in-vitro and in-vivo evaluation. Drug Dev Ind Pharm. 2023;49(9):580–9.
47. Patel R, Patel H, Baria A. Formulation and evaluation of carbopol gel containing liposomes of ketoconazole. (Part-II) Int J Drug Deliv Technol. 2009;1: (2):42–5.
48. Khullar R, Kumar D, Seth N, Saini S. Formulation and evaluation of mefenamic acid emulgel for topical delivery. SPJ. 2012;20(1):63–7.
49. Hossain ML, Hammer K, Lim LY, Hettiarachchi D, Locher C. Optimisation of an agar overlay assay for the assessment of the antimicrobial activity of topically applied semi-solid antiseptic products including honey-based formulations. J Microbiol Methods. 2022;202:106596.
50. Magaldi S, Mata-Essayag S, Hartung de Capriles C, Perez C, Colella MT, Olaizola C, et al. Well diffusion for antifungal susceptibility testing. IJID. 2004;8(1):39–45.
51. Tenover FC. Antibiotic susceptibility testing. In: Schaechter M, editor. Encyclopedia of microbiology, 3rd ed. Oxford, UK: Academic Press; 2009. p. 67–77.
52. Gharaghani M, Rezaei-Matehkolaei A, Zarei Mahmoudabadi A, Keikhaei B. The frequency, antifungal susceptibility and enzymatic profiles of Candida species isolated from neutropenic patients. Jundishapur J Microbiol. 2016;9(11):41446.
53. Taghipour S, Rezaei-Matehkolaei A, Zarei MA. Antifungal susceptibility profiles of Candida species isolated from Ahvaz Jundishapur Educational Hospitals. Jundishapur J Microbiol. 2018;11(2):e78851.
54. Abdel-Rashid RS, Helal DA, Alaa-Eldin AA, Abdel-Monem R. Polymeric versus lipid nanocapsules for miconazole nitrate enhanced topical delivery: in vitro and ex vivo evaluation. Drug Deliv. 2022;29(1):294–304.
55. Ahmed AM, Ibrahim MW, Mohamad AA. Application of HPLC method in determination of miconazole nitrate in environmental samples from El Gharbia governorate in Egypt. J Anal Pharm Res. 2019;8(4):160–4.
56. Hermawan D, Suwandri SU, Istiqomah A, Aboul-Enein HY. Development of high performance liquid chromatography method for miconazole analysis in powder sample. IOP Conf Ser Mater Sci Eng. 2017;172:012011.
57. Elhabak M, Ibrahim S, Abouelatta SM. Topical delivery of ascorbic acid spanlastics for stability enhancement and treatment of UVB induced damaged skin. Drug Deliv. 2021;28(1):445–53.
58. Danaei M, Dehghankhold M, Ataei S, Hasanzadeh Davarani F, Javanmard R, Dokhani A, et al. Impact of particle size and polydispersity index on the clinical applications of lipidic nanocarrier systems. Pharmaceutics. 2018;10(57):1–17.
59. Salama HA, Mahmoud AA, Kamel AO, Abdel Hady M, Awad GAS. Brain delivery of olanzapine by intranasal administration of transfersomal vesicles. J Liposome Res. 2012;22(4):336–45.
60. Fahmy AM, El-Setouhy DA, Habib BA, Tayel SA. Enhancement of transdermal delivery of haloperidol via spanlastic dispersions: entrapment efficiency vs. particle size. AAPS PharmSciTech. 2019;20(3):1–13.
61. Elazreg R. Formulation and in vitro evaluation of methazolamide elastic vesicular systems. AJPS. 2014;49(1):75–84.
62. Abdelrahman FE, Elsayed I, Gad MK, Elshafeey AH, Mohamed MI. Response surface optimization, ex vivo and in vivo investigation of nasal spanlastics for bioavailability enhancement and brain targeting of risperidone. Int J Pharm. 2017;530(1-2):1–11.
63. Abdelbary G, El-Gendy N. Niosome-Encapsulated gentamicin for ophthalmic controlled delivery. AAPS PharmSciTech. 2008;9(3):740–7.

64. Kelemen H, Hancu G, Gâz-Florea SA, Nemes-Nagy E, Papp LA, Mircia E. Characterization of inclusion complexes between miconazole and different cyclodextrin derivatives. Acta Med Marisiensis. 2018;64(2):70–6.
65. Jayachandran P, Ilango S, Suseela V, Nirmaladevi R, Shaik MR, Khan M, et al. Green synthesized silver nanoparticle-loaded liposome-based nanoarchitectonics for cancer management: in vitro drug release analysis. Biomedicines. 2023;11(1):217.
66. Loo C-Y, Gnanaraj C, Traini D, Young PM, Lee W-H. Fabrication of polyphenol nanoparticles co-stabilized with different polyvinylpyrrolidone concentrations: effects on particle stability, drug release and cellular uptake. J Drug Deliv Sci Technol. 2023;85(104574):1–13.
67. Ribes S, Fuentes A, Talens P, Barat JM, Ferrari G, Donsì F. Influence of emulsifier type on the antifungal activity of cinnamon leaf, lemon and bergamot oil nanoemulsions against Aspergillus niger. Food Control. 2017;73(48):784–95.
68. Nielsen CK, Kjems J, Mygind T, Snabe T, Meyer RL. Effects of tween 80 on growth and biofilm formation in laboratory media. Front Microbiol. 2016;7:1878.
69. ElMeshad AN, Mohsen AM. Enhanced corneal permeation and antimycotic activity of itraconazole against *Candida albicans* via a novel nanosystem vesicle. Drug Deliv. 2016;23(7):2115–23.
70. Marques SM, Chavan DU, Bhide PJ, Joshi M, Kumar L, Shirodkar RK. Novel luliconazole spanlastic nanocarriers: development and characterisation. Curr Drug Deliv. 2023;20(6):792–806.
71. Shirsand S, Kanani K, Keerthy D, Nagendrakumar D, Para M. Formulation and evaluation of ketoconazole niosomal gel drug delivery system. Int J Pharm Investig. 2012;2(4):201–7.
72. Aziz D, Mohamed SA, Tayel S, Makhlouf A. Enhanced ocular anti-aspergillus activity of tolnaftate employing novel cosolvent-modified spanlastics: formulation, statistical optimization, kill kinetics, ex vivo trans-corneal permeation, in vivo histopathological and susceptibility study. Pharmaceutics. 2022;14(8):1746.
73. Caldeirão ACM, Araujo HC, Arias LS, Ramírez Carmona W, Miranda GP, Oliveira SHP, et al. Nanocarriers of miconazole or fluconazole: effects on three-species Candida biofilms and cytotoxic effects in vitro. J Fungi. 2021;7(7):500.
74. Lam P-L, Wong M-M, Hung L-K, Yung L-H, Tang JC-O, Lam K-H, et al. Miconazole and terbinafine induced reactive oxygen species accumulation and topical toxicity in human keratinocytes. Drug Chem Toxicol. 2022;45(2):834–8.
75. Kim H, Jung S, Yeo S, Kim D, Na YC, Yun G, et al. Characteristics of skin deposition of itraconazole solubilized in cream formulation. Pharmaceutics. 2019;11(4):195.